NEURODEGENERATION

Reelin protects against amyloid β toxicity in vivo

Courtney Lane-Donovan,[1,2,3]* Gary T. Philips,[4] Catherine R. Wasser,[1,3] Murat S. Durakoglugil,[1,3] Irene Masiulis,[1] Ajeet Upadhaya,[1,3] Theresa Pohlkamp,[1,3,5] Cagil Coskun,[1] Tiina Kotti,[1] Laura Steller,[6] Robert E. Hammer,[7] Michael Frotscher,[6] Hans H. Bock,[8] Joachim Herz[1,2,3,5,9]*

Alzheimer's disease (AD) is a currently incurable neurodegenerative disorder and is the most common form of dementia in people over the age of 65 years. The predominant genetic risk factor for AD is the ε4 allele encoding apolipoprotein E (ApoE4). The secreted glycoprotein Reelin enhances synaptic plasticity by binding to the multifunctional ApoE receptors apolipoprotein E receptor 2 (Apoer2) and very low density lipoprotein receptor (Vldlr). We have previously shown that the presence of ApoE4 renders neurons unresponsive to Reelin by impairing the recycling of the receptors, thereby decreasing its protective effects against amyloid β (Aβ) oligomer–induced synaptic toxicity in vitro. We showed that when Reelin was knocked out in adult mice, these mice behaved normally without overt learning or memory deficits. However, they were strikingly sensitive to amyloid-induced synaptic suppression and had profound memory and learning disabilities with very low amounts of amyloid deposition. Our findings highlight the physiological importance of Reelin in protecting the brain against Aβ-induced synaptic dysfunction and memory impairment.

INTRODUCTION

Alzheimer's disease (AD) is a progressive neurodegenerative disease characterized by the buildup of plaques of amyloid β (Aβ) and neurofibrillary tangles of hyperphosphorylated tau. An early-onset form of AD is caused by familial mutations in the Aβ-generating machinery and accounts for a small percentage of patients. The primary genetic risk factor for the far more common late-onset form of AD is possession of the ε4 allele encoding apolipoprotein E (ApoE4), which is present in 20% of the population but has a prevalence of 50 to 80% in AD patients (*1*).

We have previously shown that ApoE4 disrupts synaptic function by impairing the recycling of apolipoprotein E receptor 2 (Apoer2) in the neuron (*2*). Apoer2, together with the very low density lipoprotein receptor (Vldlr), also binds the protein Reelin, a large secreted neuromodulator that regulates central nervous system (CNS) development and enhances synaptic plasticity (*3*, *4*). Reelin clusters Apoer2 and Vldlr, leading to the activation of the cytosolic adaptor protein Disabled-1 (Dab1), which has several important consequences (*3*, *5*). First, Dab1 activation leads to the phosphatidylinositol 3-kinase–dependent inhibition of glycogen synthase kinase 3β (GSK3β), which results in the dephosphorylation of the microtubule-associated protein tau (*3*, *6*). Second, Dab1-mediated activation of Src family kinases leads to the tyrosine phosphorylation of the NR2 subunit of *N*-methyl-D-aspartate receptors (NMDARs), resulting in reduced NMDAR endocytosis and greater calcium influx when NMDARs are activated (*7*–*10*). Consequently, Reelin application to acutely isolated hippocampal slices enhances long-term potentiation (LTP) (*11*). On the other hand, direct application of Aβ oligomers to slices inhibits LTP, which can be prevented by co-application of Reelin (*12*, *13*). Because ApoE4 reduces the availability of Reelin receptors at the synaptic surface by impairing receptor recycling, Reelin cannot effectively protect against the Aβ-mediated impairment of synaptic plasticity in the presence of ApoE4 (*2*). Consistent with this, intrathecal injection of Reelin strengthens learning and memory (*14*). Moreover, nonphysiological overexpression of Reelin delays plaque deposition and memory impairment in a transgenic mouse model (*15*). However, there has been no in vivo evidence to show that activation of the Apoer2 signaling pathway by Reelin protects the brain against the pathological consequences of rising amyloid accumulation in AD.

In addition to its roles in adult synaptic function, Reelin is expressed early in development by Cajal-Retzius cells and directs the positioning of postmitotic neurons (*16*). Reelin knockout (*reeler*) mice have inverted cortical layering, disrupted hippocampal structure, and a lack of foliation in the cerebellum, which leads to a severe ataxic phenotype and early lethality (*17*, *18*). Heterozygous *reeler* mice have normal neuronal migration but exhibit reduced LTP, impaired learning, and reduced sensorimotor gating (*19*, *20*). It remains unclear if the phenotype in the heterozygous *reeler* mouse is due to the developmental or adult effects of Reelin deficiency, for example, subtle neuroanatomical and/or morphological changes or defects in synaptic transmission.

To address these fundamental questions, we have investigated the effect of complete Reelin loss on synaptic function and behavior in normal mice and in mice that moderately overproduce Aβ. To bypass the deleterious consequences of embryonic absence of Reelin for brain development, we generated an inducible conditional Reelin knockout (cKO) mouse. After Reelin inactivation at 2 months of age, Reelin cKO mice were morphoanatomically indistinguishable from their wild-type littermate controls with a normal cortical architecture, but they did exhibit a subtle behavioral and electrophysiological phenotype. However, modest transgenic expression of human Aβ in these mice resulted in impaired spatial learning and memory. Together, our results suggest that, whereas a healthy adult CNS

[1]Department of Molecular Genetics, University of Texas Southwestern Medical Center, Dallas, TX 75390, USA. [2]Department of Neuroscience, University of Texas Southwestern Medical Center, Dallas, TX 75390, USA. [3]Center for Translational Neurodegeneration Research, University of Texas Southwestern Medical Center, Dallas, TX 75390, USA. [4]Center for Neural Science, New York University, New York, NY 10003, USA. [5]Center for Neuroscience, Department of Neuroanatomy, Albert-Ludwigs-University, Freiburg 79085, Germany. [6]Institute for Structural Neurobiology, Center for Molecular Neurobiology, Hamburg 20251, Germany. [7]Department of Biochemistry, University of Texas Southwestern Medical Center, Dallas, TX 75390, USA. [8]Clinic for Gastroenterology, Hepatology and Infectiology, Heinrich-Heine-University, Düsseldorf 40225, Germany. [9]Department of Neurology and Neurotherapeutics, University of Texas Southwestern Medical Center, Dallas, TX 75390, USA.
*Corresponding author. E-mail: joachim.herz@utsouthwestern.edu (J.H.); courtney.lane@utsouthwestern.edu (C.L.-D.)

can compensate for Reelin loss, Reelin signaling is vital to protect against the incipient Aβ toxicity that induces synaptic dysfunction during the early stages of aging.

RESULTS

Conditional knockout mice exhibit complete loss of Reelin upon tamoxifen induction and recapitulate the reeler phenotype when induced in the germline

To determine the role of Reelin in adult synapse function and behavior, we first had to separate the adult effects of Reelin loss from its absolute requirement for brain development. Because Reelin-deficient (*reeler*) mice have a severe developmental phenotype that effectively compromises all studies of Reelin loss in the adult brain (*18*), we generated a Reelin cKO mouse line. *Reln*$^{flox/flox}$ mice were derived using a construct in which the first exon of the *Reln* gene was flanked with loxP sites (Materials and Methods and Fig. 1A), bred to homozygosity, and crossed with an inducible Cre recombinase–expressing line, from here on referred to as the CAG-Cre^{ERT2} line (*21*). This mouse line ubiquitously expresses a fusion protein composed of Cre recombinase and a mutated form of the estrogen receptor (Cre-ERT2), and tamoxifen administration induces nuclear Cre activity and knockout of the floxed gene. Western blotting showed that Reelin amounts in the hippocampi of tamoxifen-injected *Reln*$^{flox/flox}$ mice were reduced to less than 5% of that in vehicle-injected mice and that Reelin was undetectable in most mice (Fig. 1, B and C). The brain-wide loss of Reelin was confirmed through immunohistochemistry, which revealed a total loss of Reelin throughout the brain (fig. S1). Reelin-induced phosphorylation of Dab1 targets this protein for proteasomal degradation, and thus, loss of Reelin signaling results in higher Dab1 protein abundance (*22*, *23*). Immunoblotting showed that Reelin cKO mice exhibited increased Dab1 protein abundance, similar to *reeler* mice and confirming complete loss of Reelin function (Fig. 1D). Moreover, this observation also confirms that the Reelin signaling pathway is physiologically active in the adult brain because Dab1 turnover depends on pathway activation.

To confirm that the *Reln*$^{flox/flox}$ line can fully recapitulate the *reeler* phenotype, we crossed *Reln*$^{flox/flox}$ mice with the Meox-Cre line, which induces recombination in epiblast-derived tissues and thus also in the germline (*24*). These mice showed the typical *reeler* phenotype with inverted cortical layering and a lack of cerebellar foliation (fig. S2). Together, these data demonstrate that Cre recombinase readily and rapidly inactivates the gene in *Reln*$^{flox/flox}$ mice, and thus, these mice constitute an effective cKO model in which the consequences of adult Reelin loss can be investigated.

Adult loss of Reelin affects the abundance of Dab1 but not that of downstream effectors or glutamate receptor

To determine the extent of the disruption of the Reelin signaling pathway in Reelin cKO mice, we next assessed the activity of downstream effectors of Dab1 signaling. We found that although *reeler* mice exhibited reduced phosphorylation of GSK3β at Ser^{9} (an inhibitory phosphorylation site) (*6*), our Reelin cKO mice showed no change relative to controls (Fig. 1E), suggesting that the increased GSK3β activity in the *reeler* mouse brain (which lacks Reelin during development) is caused and maintained by the persistent disruption of the brain architecture. We similarly observed no changes in the phosphorylation of Akt, extracellular signal–regulated kinase (ERK), or Src (Fig. 1, F to H), three other downstream effectors of Reelin signaling, including in the germline *reeler* mice that survive to 2 months of age (*25*, *26*). We then determined the whole-cell abundance of glutamate receptors because these are altered in heterozygous reeler mice (*27*). GluA1 and GluA2/3 abundance was unaltered in all mice (Fig. 1, I and J). NR2A abundance was similar in all mice (Fig. 1K). NR2B abundance was increased in *reeler* mice but not in the cKO mice (Fig. 1L).

Tau is hyperphosphorylated in *reeler* mice, which likely contributes to neuronal dysfunction in these mice (*3*). We examined the phosphorylation of tau at two sites in the cKO mice: the AT8 epitope and Thr^{231}. Neither was altered in the cKO or the *reeler* mice (Fig. 1M). We further showed previously that strain background–dependent tau phosphorylation correlates with early postnatal death in these lines, which readily explains the absence of tau phosphorylation in adult *reeler* mice (*28*). Together, these biochemical results indicate that, whereas we successfully disrupted Reelin signaling in the cKO mice, other adaptive responses may be able to compensate to some extent for Reelin loss in young, healthy mice.

Adult Reelin cKO mice have normal CNS architecture

Reelin is required for the development of layered brain structures, particularly for cortical lamination and the formation of the cerebellum. Moreover, disruptions of the Reelin signaling pathway have been shown to cause granule cell dispersion (*29*). To confirm that we were successful in bypassing the severe developmental effects of Reelin gene disruption, we evaluated sections from Reelin cKO mice for altered cytoarchitecture. *reeler* mice have disorganized cortical layering; by contrast, the cKO mice exhibited normal cortical layering, as judged by NeuN labeling, 1 month after tamoxifen injection (Fig. 2, A to C). Similarly, whereas *reeler* mice have a loss of foliation in the cerebellum, cKO mice cerebella appeared grossly normal (Fig. 2, D to F), as did the hippocampi (Fig. 2, G to I). These data suggest that Reelin is not required for the maintenance of CNS layering in the adult.

After normal development, interference with Reelin signaling through application of the CR-50 antibody causes granule cell dispersion (*30*), yet we found no evidence of granule cell dispersion in Reelin cKO mice 1 month after tamoxifen injection (Fig. 2J). This discrepancy may be explained by the fact that CR-50 blocks the oligomerization of Reelin, which interferes with signaling through the canonical Reelin pathway, but may not prevent the binding of Reelin to other receptors, such as members of the Eph/Ephrin family or integrins, thereby potentially causing dominant negative interference (*31*–*33*). Moreover, injection of the functionally neutralizing CR-50 into the dentate gyrus may effectively establish a Reelin signaling gradient, leading to the dispersion; in our model, Reelin is homogenously knocked out, thus preventing the development of such a gradient.

Finally, because primary cultures of *reeler* neurons have reduced spine density and Reelin supplementation increases dendritic spine density (*14*, *34*), we measured dendritic spine density in the cKO mice. Brains were stained using the Golgi method, and the spine density of apical CA1 dendrites was measured. We found no differences between cKO and control dendritic spine density (Fig. 2, K to N). Moreover, whereas heterozygous *reeler* mice have altered spine morphology (*35*), we observed no difference in cKO mice (Fig. 2, O and P). Together, these data indicate that interruption of Reelin signaling in the adult and fully formed brain results in no obvious structural changes.

Reelin cKO mice have a mild behavioral phenotype

Because we found that adult loss of Reelin has no effect on brain structure, we sought to explore the behavioral phenotypes of Reelin cKO mice. *Reeler* mice have a stereotypical ataxia, which precludes equal comparison with wild-type mice on most behavioral tasks. Moreover, heterozygous *reeler* mice have an age-dependent reduction in ability to perform the rotarod task (*36*). To determine whether adult loss of Reelin affects motor skills, we tested motor learning and coordination in 3-month-old Reelin cKO mice on the rotarod. We found no difference in the performance of cKO mice compared to their littermate controls over the course of 10 days of training (fig. S3A).

Next, we evaluated Reelin cKO mice for changes in anxiety because heterozygous *reeler* mice have reduced anxiety (*37*). First, mice were tested on the open-field task, in which they were put into an open-field box, and the time spent in the center versus the periphery was measured. Reelin cKO mice spent slightly more time than did controls toward the end of the hour in the center of the field compared to the periphery, which may suggest reduced anxiety (Fig. 3A). To further evaluate this potential reduced anxiety phenotype, we tested the mice on the elevated plus maze task. In this task, mice were placed on an elevated central platform and allowed to explore the four arms extending from it: two "closed" arms with high walls and two "open" arms with no walls. More time spent in the closed arm is considered to reflect increased anxiety. We found that all genotypes spent similar

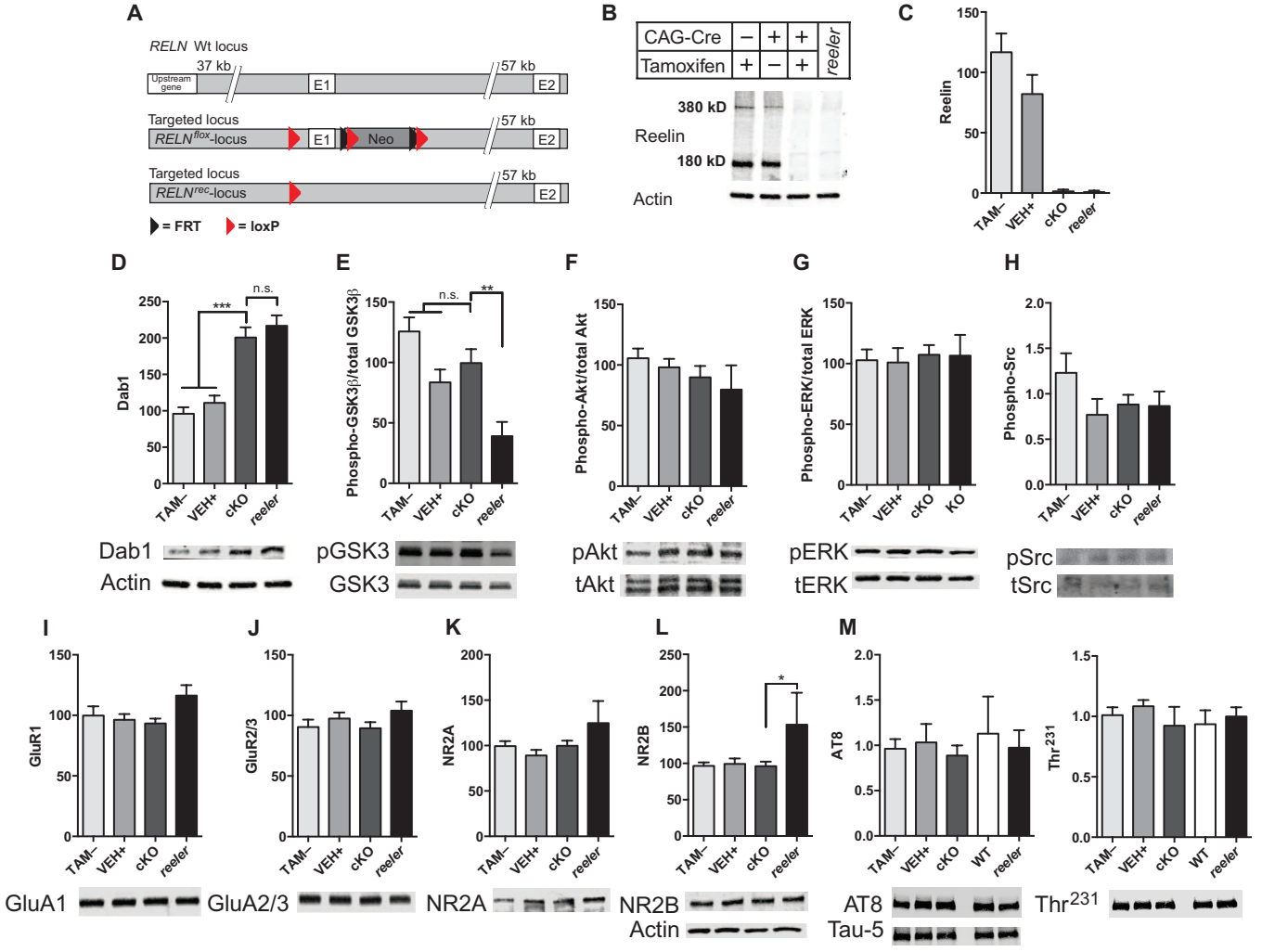

Fig. 1. Adult loss of Reelin causes increased Dab1 abundance without changing the abundance of downstream effectors or glutamate receptors. (**A**) *Reln*$^{flox/flox}$ mice were generated by flanking exon 1 of the *Reln* gene with loxP sites. The mice were bred to homozygosity and crossed with the CAG-Cre^{ERT2} line, which ubiquitously expresses a tamoxifen-inducible Cre recombinase. (**B**) Western blot of whole hippocampal lysates with G10 antibody, demonstrating inducible Reelin knockout. The positions of the180- and 380-kD Reelin forms are indicated. TAM–, tamoxifen-injected *Reln*$^{flox/flox}$ mouse; VEH+, vehicle-injected CAG-Cre^{ERT2}:*Reln*$^{flox/flox}$ mouse; cKO, tamoxifen-injected CAG-Cre^{ERT2}:*Reln*$^{flox/flox}$ mouse. (**C**) Quantification of 180-kD Reelin band Western blotting. Data are presented as means ± SEM (TAM–, VEH+, n = 10 mice; cKO, n = 11 mice; *reeler*, n = 4 mice). (**D** to **M**) Whole hippocampal lysates from mice of the indicated genotypes were evaluated by Western blot. Total Dab1 abundance normalized to actin [same samples as in (B)] (D) [one-way analysis of variance (ANOVA), $P < 0.0001$; post hoc TAM– compared to cKO, $P < 0.001$; VEH+ compared to cKO, $P < 0.001$; n.s., not significant] (TAM–, n = 11 mice; VEH+, n = 12 mice; cKO, n = 12 mice; *reeler*, n = 7 mice); phosphorylated (p) GSK3β (Ser^{9}) normalized to total GSK3β (E) (one-way ANOVA, P = 0.0012; post hoc cKO compared to KO, $P < 0.001$); phosphorylated Akt normalized to total (t) Akt (F); phosphorylated ERK normalized to total ERK (G); phosphorylated Src normalized to total Src (H); GluA1 (I); GluA2/3 (J); NR2A (K) (one-way ANOVA, $P_{pAkt/tAkt}$ = 0.5329, $P_{pERK/tERK}$ = 0.9946, P_{pSrc} = 0.2660, P_{GluR1} = 0.1458, $P_{GluR2/3}$ = 0.3996, P_{NR2A} = 0.1168); and NR2B (L) (one-way ANOVA, P = 0.0593; post hoc cKO compared to *reeler*, $P < 0.05$). For (E) to (G) and (I) to (L): TAM–, n = 8 mice; VEH+, n = 11 mice; cKO, n = 11 mice; *reeler*, n = 5 mice. For (H): TAM–, n = 6 mice; VEH+, n = 6 mice; cKO, n = 6 mice; *reeler*, n = 5 mice. Phosphorylated tau normalized to total tau (M) (one-way ANOVA, P_{AT8} = 0.9610, P_{Thr231} = 0.7995; n = 4 mice per genotype) is also shown. All samples in (D) to (L) were normalized to actin or RAP and then to the control (TAM– and VEH+) mice. Data are presented as means ± SEM.

amounts of time in the closed arm (fig. S3B). Together, these two measures of anxiety suggest that Reelin cKO mice have low hypoanxiety that emerges with time.

In addition to anxiety and motor deficits, heterozygous *reeler* mice have reduced prepulse inhibition (PPI), which is an indication of disrupted sensorimotor gating (*20*). We tested PPI in the cKO mice, which had normal startle amplitudes in response to tones ranging from 70 to 120 dB (fig. S3C), at three prepulse tones: 74, 78, and 86 dB. Surprisingly, Reelin cKO mice showed no alterations in PPI at 74 and 86 dB, with a significant, though only slight, increase in PPI at 78 dB (Fig. 3B). Together, these mild phenotypes suggest that the anxiety and sensorimotor deficits found in heterozygous *reeler* mice are caused by the loss of developmental functions of Reelin, and further validate the importance of the cKO model for understanding the roles of Reelin in the adult and aging brain.

Reelin cKO mice have no deficits in learning and memory

Given the mild phenotype on anxiety and sensorimotor tests in these mice, we wondered about the effect of Reelin loss on learning and memory. Reelin modulates learning and memory; notably, heterozygous *reeler* mice are impaired on some memory tasks, and intraventricular injection of Reelin enhances Morris water maze performance (*14*, *15*, *19*). To investigate the role of Reelin in adult memory acquisition, we subjected 3-month-old cKO mice to the Morris water maze and fear conditioning tasks. First, in the Morris water maze, mice were trained to find a platform hidden in cloudy water over the course of 10 days, followed by a 60-s probe trial on day 11, in which the platform was removed. Reelin cKO mice showed no differences in acquisition of the platform location (Fig. 3C) and a similar preference for the target quadrant during the probe trial (Fig. 3D). Next, mice were tested for alterations in fear learning with contextual and cued fear conditioning. Similar to the Morris water maze results, cKO mice showed normal acquisition and memory in both contextual (fig. S3D) and cued fear conditioning (fig. S3E).

Reelin cKO mice have enhanced LTP

Given that Reelin cKO mice are virtually indistinguishable from wild-type littermates by biochemical and behavioral assessments, we wanted to determine whether there were any differences in neuronal function, specifically synaptic plasticity. Because Reelin application enhances θ-burst LTP, and heterozygous *reeler* mice have reduced LTP, we hypothesized that LTP in Reelin cKO mice would be reduced. To investigate the electrophysiological effects of Reelin loss, we performed θ-burst LTP experiments on acutely isolated hippocampal slices from 7-month-old cKO mice. Briefly, we recorded field excitatory postsynaptic potentials (fEPSPs) from CA1 dendrites after stimulating afferent CA3 axons (Schaeffer collaterals) and compared the fEPSP slope before and after θ-burst stimulation (Fig. 3E). Although initial LTP (0 to 20 min) was the same between control and cKO mice (Fig. 3F), the late component of LTP (between 40 and 60 min) in cKO mice was increased nearly 50% compared to control mice (Fig. 3G). Input-output curves were similar between the two genotypes, suggesting that the LTP change was not caused by differences in baseline synaptic transmission (Fig. 3H). These electrophysiological results suggest that, although Reelin cKO mice appear normal according to standard behavioral tests, the electrophysiology of their hippocampi is altered.

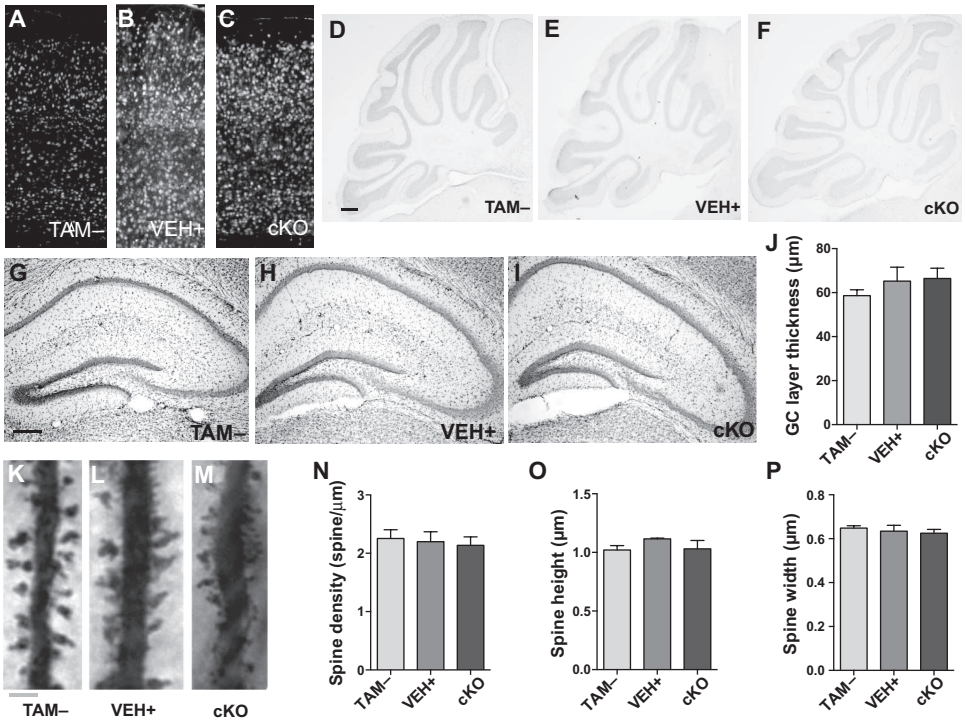

Fig. 2. Adult Reelin cKO mice have normal architecture, no granule cell dispersion, and no alterations in dendritic spine density or morphology. (**A** to **P**) Sections were compared from TAM– (A, D, G, and K), VEH+ (B, E, H, and L), and cKO (C, F, I, and M) mice. Cortical sections were evaluated for disrupted layering by NeuN immunohistochemistry (A to C). Scale bar, 200 μm. Cerebellar (D to F) (scale bar, 200 μm) and hippocampal (G to I) (scale bar, 200 μm) sections were stained with cresyl violet. The granule cell layer thickness was measured to assess granule cell (GC) dispersion (J) (one-way ANOVA, $P = 0.5016$). For (A) to (F), $n = 3$ sections per mice, 3 mice per genotype. For (G) to (J), $n = 6$ sections per mice, 3 mice per genotype. Golgi-stained CA1 apical dendrites (K to M) were analyzed for changes in spine density (N) and spine morphology (O and P) (scale bar, 5 μm) (one-way ANOVA, $P_{Density} = 0.8681$, $P_{Height} = 0.4822$, $P_{Width} = 0.7753$) (TAM–, $n = 38$; VEH+, $n = 29$; cKO, $n = 25$, where n represents total neurons analyzed from three mice per genotype). Data are presented as means ± SEM.

Reelin loss does not accelerate plaque deposition or increase Aβ amounts in Tg2576 mice

The changes in synaptic plasticity in Reelin cKO mice raised the possibility that these mice might be more sensitive to toxicity induced by Aβ oligomers. We have previously shown that Reelin directly protects against Aβ toxicity at the synapse in acutely isolated hippocampal slices (*12*). Despite the mild behavioral and synaptic alterations in Reelin cKO mice, we suspected that adult loss of Reelin might exacerbate this Aβ toxicity. To investigate the in vivo consequences of Reelin loss on Aβ toxicity, we crossed the Reelin cKO line with the Tg2576 (APPSwe) AD model mouse line, which overexpresses

a mutant form of amyloid precursor protein (APP) bearing the Swedish mutation (KM670/671NL), resulting in increased Aβ amounts starting around 4 months of age (*38*).

Aβ concentration may correlate with cognitive decline (*39*), and Reelin haploinsufficiency increases Aβ abundance and accelerates plaque development in one particular strain of mutant APP transgenic mice (*40*). We

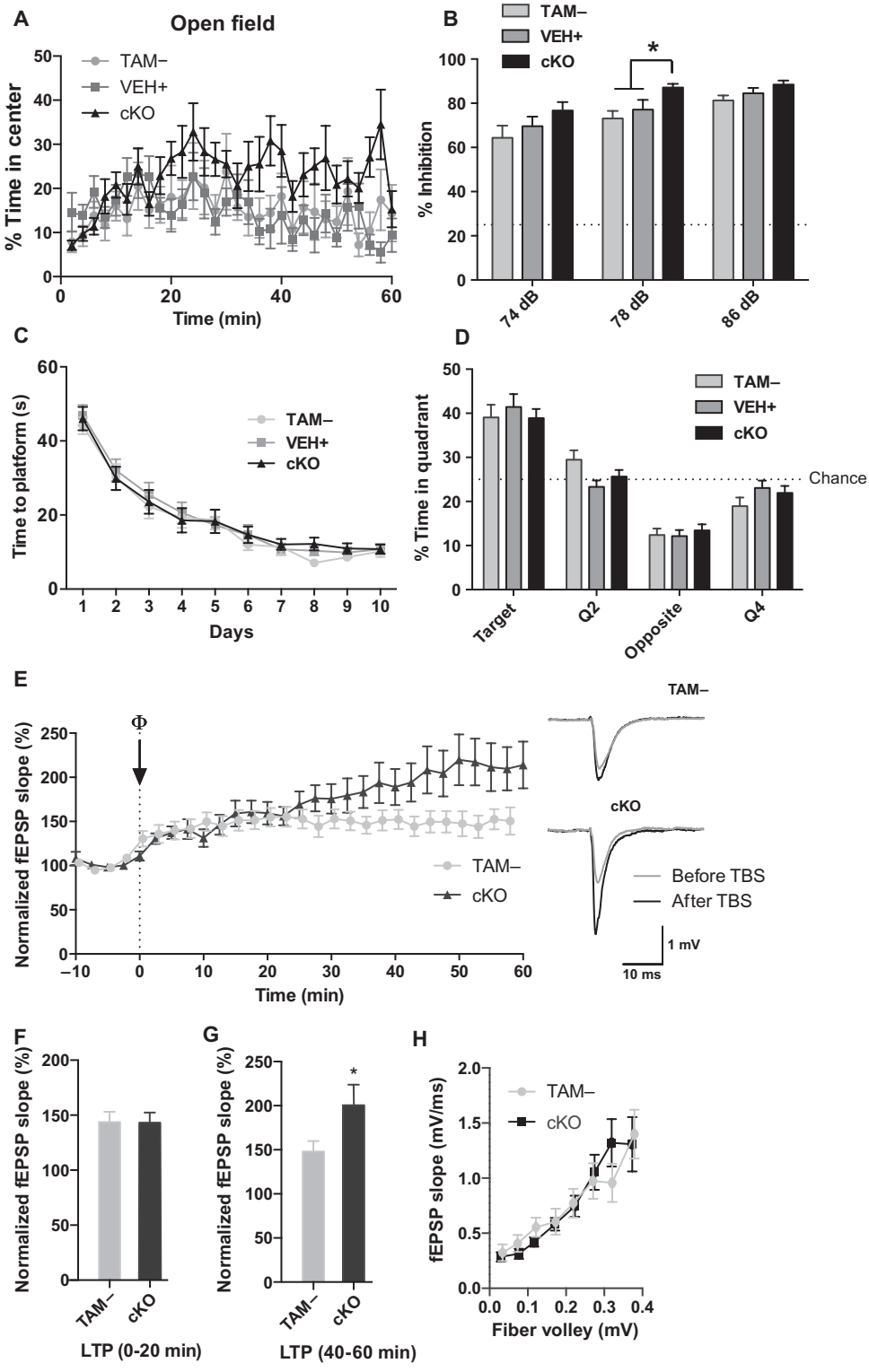

Fig. 3. Reelin cKO mice have mild behavioral changes and increased LTP. (A to D) Reelin cKO mice have hypoanxiety and mildly enhanced PPI, but no changes in learning. (A) The percent time mice spent in the center of an open-field apparatus for each 2-min bin is shown. A two-way repeated-measures ANOVA shows a strong effect of time ($P < 0.001$), a nonsignificant trend of genotype ($P = 0.0783$), and a significant interaction between the two ($P = 0.0129$) (TAM–, $n = 11$ mice; VEH+, $n = 10$ mice; cKO, $n = 14$ mice). (B) Mice were tested for PPI with the indicated tones preceding a 120-dB tone. Data shown are reduction of startle at each prepulse relative to the startle when no prepulse was played before the 120-dB tone (two-way ANOVA, $P_{Interaction} = 0.876$, $P_{Prepulse\ intensity} < 0.0001$, $P_{Genotype} = 0.0008$; post hoc at 78 dB: TAM– compared to cKO, $P = 0.0013$; VEH+ compared to cKO, $P = 0.0306$) (TAM–, $n = 16$ mice; VEH+, $n = 18$ mice; cKO, $n = 17$ mice). (C and D) Morris water maze results from cKO mice. The latency of mice to find a hidden platform over a 10-day training period was measured (C) (two-way repeated-measures ANOVA, $P_{Interaction} = 0.9993$, $P_{Time} < 0.0001$, $P_{Genotype} = 0.5616$; $n = 10$ per group). On the 11th day, the platform was removed, and the time spent in the quadrant (Q) that had previously contained the platform was measured (D) (two-way ANOVA, $P_{Genotype} > 0.999$, $P_{Quadrant} < 0.0001$, $P_{Interaction} = 0.1874$) (TAM–, $n = 16$ mice; VEH+, $n = 17$ mice; cKO, $n = 17$ mice). (E to H) Reelin cKO mice have enhanced late LTP. (E) Field recordings were made from the stratum radiatum of the CA1 region of hippocampal slices from 7-month-old Reelin cKO mice before and after application of θ-burst stimulation–induced LTP. Every 2 min were averaged for analysis. Sample traces are shown before and after θ-burst stimulation (TBS) (right). (F and G) The average LTP at 0 to 20 min was similar between control and cKO mice (F) (unpaired *t* test, $P = 0.9511$). At 40 to 60 min, cKO mice had increased LTP (G) (unpaired *t* test, $P = 0.0483$). (H) The input-output curves were unaltered between cKO and control mice (unpaired *t* test, $P = 0.9828$) (TAM–, $n = 15$ slices from 6 mice; cKO, $n = 11$ slices from 4 mice). Data are presented as means ± SEM.

therefore investigated whether adult Reelin deficiency accelerated plaque development in mice injected with tamoxifen or vehicle at 2 months of age and aged for 5 months. To quantify amyloid plaque formation, we performed immunohistochemistry for Aβ using the 4G8 antibody (*41*) in 7-month-old mice and found a lack of plaques in the cortex in these mice (Fig. 4, A and B). As a positive control for our immunostaining, we also stained brain sections from a 9-month-old APP/PS1 transgenic mouse, which showed readily detectable plaque deposition (Fig. 4C). We next quantified the phosphate-buffered saline (PBS)–soluble (monomers) and PBS-insoluble (fibrillar) Aβ in the brains of Tg2576:Reelin cKO and Tg2576 control (TAM−) mice by Western blot. Aβ abundance was low but detectable in Tg2576 mice but varied widely among all the genotypes, and we found no significant difference between Tg2576:Reelin cKO and Tg2576 mice in either the soluble or insoluble fractions (Fig. 4D). Quantification of the species of Aβ present by enzyme-linked immunosorbent assay (ELISA) also revealed no difference in the amount of PBS-soluble or PBS-insoluble $Aβ_{40}$ or $Aβ_{42}$ (Fig. 4E).

Reelin loss accelerates cognitive impairment in Tg2576 mice

Next, we explored if Reelin loss left mice susceptible to amyloid toxicity. Seven-month-old cKO mice were tested in the Morris water maze. At this age, Tg2576 mice accumulate minute amounts (less than 10 pmol/g) of Aβ, and cognitive deficits in the Morris water maze are typically not detectable until Aβ concentrations are more than a hundred-fold higher (*42*). Morris water maze testing revealed that Tg2576 mice demonstrated normal learning and memory at this age as expected, whereas Tg2576:Reelin cKO mice showed severely impaired acquisition and performance on the probe trial equivalent to chance (Fig. 5, A and B). There was no difference in swim speed (Fig. 5C), indicating that the impairment was caused by a hippocampal-dependent learning and memory deficit and not a sensorimotor defect. To confirm that the impairment was not due to an age-dependent effect of Reelin loss, we tested naïve 7-month-old Reelin cKO mice in the Morris water maze and found that they performed as well as the wild type (fig. S4). These data thus provide direct evidence that Reelin protects against memory impairment caused by Aβ toxicity.

Tg2576:Reelin cKO mice do not have increased LTP

To determine how the presence of Aβ affected the increased late component of LTP in cKO slices, we assessed hippocampal synaptic plasticity in Tg2576:Reelin cKO mice and Tg2576 control brains. Because all four genotypes were recorded in parallel, the cKO and TAM− measurements are recast from Fig. 3. Quantification of θ-burst stimulation–induced LTP indicated that the increased late component of LTP in Reelin cKO slices was abolished in Tg2576:Reelin cKO slices (Fig. 5, D to F). These results show that Aβ affects synaptic responses to a greater extent in Reelin cKO mice than in control mice, which mirrors the cognitive impairment elicited by low amounts of Aβ in these mice.

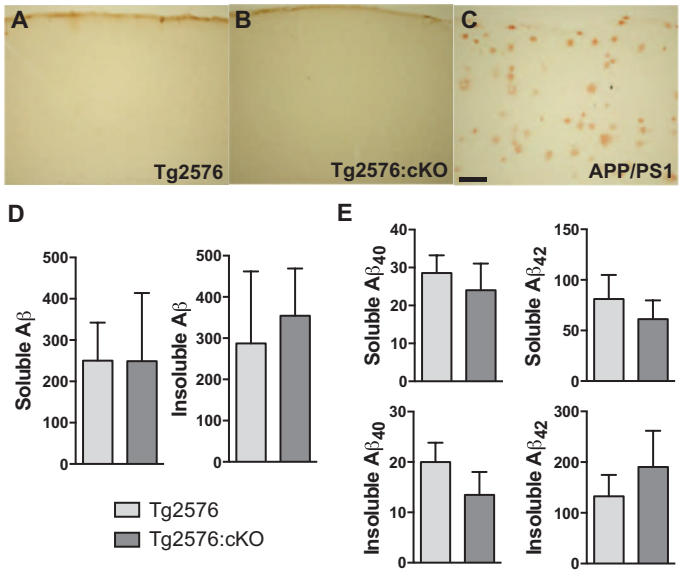

Fig. 4. Loss of Reelin does not accelerate amyloid pathology in 7-month-old Tg2576 mice. (A and B) Immunohistochemistry with 4G8 antibody was performed on brains of (A) Tg2576 and (B) Tg2576:cKO mice to evaluate plaque deposition (n = 3 mice per genotype). (C) Nine-month-old APP/PS1 mice were used as a positive control because they had no obvious plaques. Scale bar, 200 μm. (D) The abundance of PBS-soluble and PBS-insoluble Aβ was measured with Western blot and quantified. No difference was observed between cKO and control mice (unpaired t test, $P_{soluble}$ = 0.9945, $P_{insoluble}$ = 0.7554) (n = 6 mice per genotype). (E) The abundance of PBS-soluble and PBS-insoluble $Aβ_{40}$ and $Aβ_{42}$ was measured by ELISA. No difference was observed between cKO and control mice (unpaired t test: $Aβ_{40}$, $P_{soluble}$ = 0.6016, $P_{insoluble}$ = 0.3398; $Aβ_{42}$, $P_{soluble}$ = 0.6116, $P_{insoluble}$ = 0.4789) (n = 9 Tg2576 mice, n = 4 Tg2576:cKO mice). Data are presented as means ± SEM.

DISCUSSION

We investigated the physiological importance of Reelin for behavior, synaptic function, and protection against Aβ toxicity in the adult brain. Using a Reelin cKO mouse model, we found that the isolated loss of Reelin had only subtle effects on neuronal physiology and function of an adult mouse. However, loss of Reelin rendered excitatory synapses susceptible to functional suppression by Aβ, which resulted in impaired learning and memory in a commonly used AD mouse model. Together, our findings provide in vivo evidence that highlights the key role of Reelin signaling for the protection against Aβ toxicity in the adult brain.

Since the identification of the *reeler* mouse phenotype (*18*) with its severe ataxic phenotype, disrupted layering in several brain regions, and early lethality, and the discovery of the Reelin gene (*17*), researchers have studied the role of Reelin in brain development, synaptic function, and neuronal disease. Several studies have pointed to a prominent role for Reelin in adult synaptic function. First, application of Reelin to acute hippocampal slices enhances θ-burst LTP (*11*). Likewise, intraventricular injection of Reelin into wild-type mice enhances learning and memory (*14*). Conversely, heterozygous *reeler* mice have reduced amounts of Reelin and deficits in both LTP and learning and memory (*19*).

Given the behavioral deficits observed in heterozygous *reeler* mice, we tested Reelin cKO mice on a battery of behavioral measures and were surprised to find that the mice were indistinguishable from their wild-type littermate controls by most parameters, except for slow-onset hypoanxiety and minor enhancement in PPI. These findings suggest that most phenotypes described in heterozygous or homozygous *reeler* mice are caused by developmental changes in the brain, and not by acute loss of Reelin signaling in the adult brain. They also stress the importance of using a cKO model to study the consequences of loss of Reelin function in the adult brain. Our findings contrast those found in mice with a postdevelopmental loss of Dab1, which is the primary cytosolic adaptor protein for Reelin. Dab1 cKO mice have a marked deficit in spatial learning (*25*). Although these behavioral differences could be explained by different mouse backgrounds, there are other possible explanations. Although they are generally

viewed as primary signaling partners, Reelin and Dab1 have various other binding partners, resulting in divergent extracellular as well as intracellular branches of several distinct signaling pathways in which Reelin and Dab1 participate and which can readily explain why loss of Reelin does not recapitulate the learning phenotype of the Dab1 cKO mice. For example, Reelin also binds to integrins, APP, and EphB receptors (*31*, *33*, *43*), and there are other ligands for the Reelin receptors, such as ApoE, ApoJ (Clusterin), and F-Spondin (*44*–*46*). Moreover, Dab1 binds to several NPXY motif–containing receptors, including APP, integrins, and LRPs (*47*–*49*). Thus, Dab1 loss may also suppress synaptic plasticity through these partners (*48*, *50*). Intriguingly, ApoJ is also a late-onset AD risk gene (*51*). Thus, the products of several AD risk genes—ApoE, ApoJ, and APP—converge on their common binding partner Apoer2 at the synapse. This convergence further emphasizes the importance of Reelin signaling through ApoE receptors and underscores the pivotal role of this ligand-receptor complex in protecting the synapse from Aβ-mediated suppression.

The *reeler* mouse shows defective neuronal migration, and disruption of Reelin signaling with CR-50, an anti-Reelin antibody, leads to granule cell dispersion (*30*). This dispersion is observed in mesial temporal lobe epilepsy (MTLE), the most common form of epilepsy (*52*). Intrahippocampal kainic acid injection causes granule cell dispersion in mice (*53*), which is associated with reduced Reelin abundance in the hippocampus (*30*). Supplementation with Reelin can prevent granule cell dispersion after kainic acid injection (*54*). We found that complete loss of Reelin in adult mice resulted in no dispersion of the granule cell layer, suggesting that additional signaling cascades are activated in response to enhanced glutamate release in MTLE and experimental kainate application, respectively, eventually leading to increased granule cell motility and dispersion (*55*).

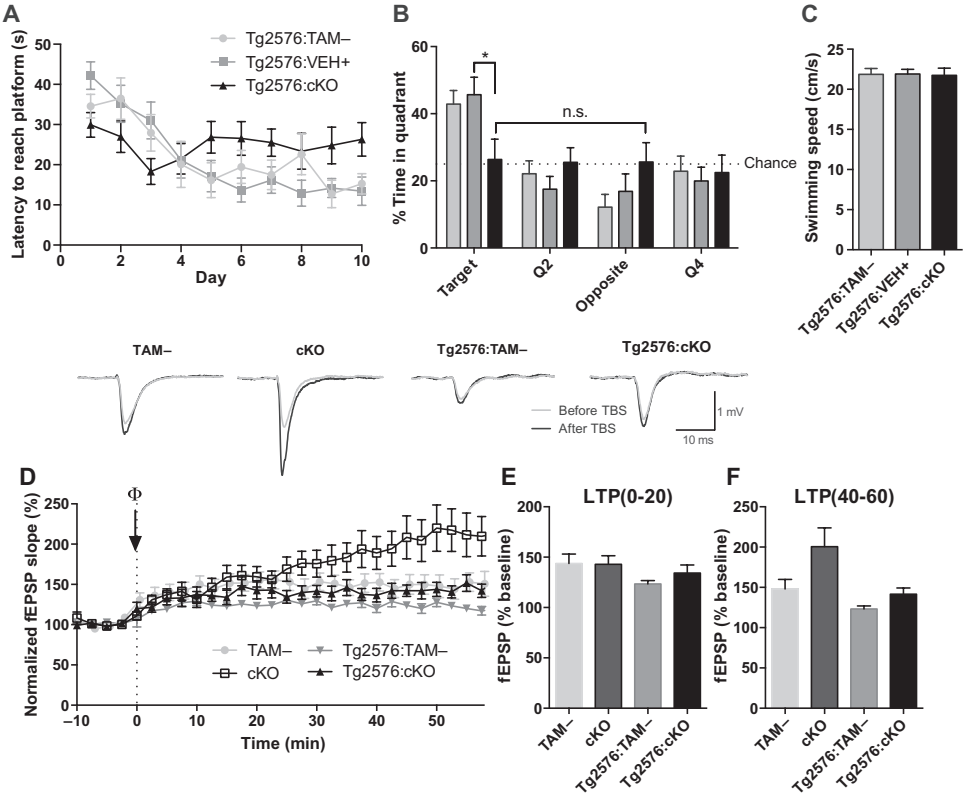

Fig. 5. Low amounts of endogenously produced Aβ induce severe memory impairment and reduce hyperexcitability in Tg2576:Reelin cKO mice. (A to C) Morris water maze testing of 7-month-old Tg2576:Reelin cKO mice showed that they had impaired acquisition of the task (A) [two-way ANOVA: $F_{18,306\ (Interaction)} = 3.370$, $P < 0.0001$, $F_{9,306\ (Time)} = 10.38$, $P < 0.0001$, $F_{2,34\ (Genotype)} = 0.564$, $P = 0.5742$] and poor performance on the probe trial (B). (C) Swim speeds between genotypes were similar (one-way ANOVA, $P = 0.9866$) (Tg2576:TAM–, $n = 9$ mice; Tg2576:VEH+, $n = 12$ mice; Tg2576:cKO, $n = 16$ mice). Data are presented as means ± SEM. (D to F) θ-Burst LTP was performed in Tg2576:Reelin cKO mice (D). No difference was observed at 0 to 20 min (E). However, at 40 to 60 min, the cKO mice had increased LTP, whereas the Tg2576:cKO mice showed similar LTP to control mice (F). One-way ANOVA revealed a significant difference at 40 to 60 min, with post hoc analyses indicating a significant difference between the cKO mice and all other genotypes ($P < 0.05$, compared to TAM–; $P < 0.01$, compared to Tg2576; $P < 0.05$, compared to Tg2576:cKO) but no difference between the other genotypes, including the Tg2576:Reelin cKO mice (TAM–, $n = 15$ slices from 6 mice; cKO, $n = 11$ slices from 4 mice; Tg2576:TAM–, $n = 11$ slices from 4 mice; Tg2576:cKO, $n = 10$ slices from 4 mice). Data are presented as means ± SEM.

Despite relatively normal behavioral and histological findings, Reelin cKO mice showed electrophysiological changes, including enhancement in the late component of LTP, in contrast to the reduced θ-burst LTP found in heterozygous *reeler* mice (*19*). Electrophysiological assessment suggests that the LTP phenotype in Reelin cKO mice is similar to that observed in ApoE4 knock-in mice, which also show enhanced LTP (*56*) and Reelin resistance, meaning a state of impaired response to endogenous or exogenously provided Reelin analogous to the impaired cellular response to insulin in type 2 diabetes (*2*). Several synaptic modifications can cause enhanced LTP. One is a change in baseline synaptic transmission, but it is unlikely to be the underlying cause because the input-output curves were similar in cKO and control mice. Another possible mechanism for enhanced LTP is reduced inhibition (*57*). Because Reelin is found primarily in inhibitory interneurons in adults, future studies will also need to focus on the effect of Reelin loss on inhibitory function. Alternatively, alterations in glutamate receptor trafficking can change excitability, and Reelin regulates glutamate receptor trafficking, thereby promoting its function, as well as synapse maturation (*34*, *58*–*60*). Finally, Reelin activation of Apoer2 initiates a transcriptional program through CREB (3′,5′-cyclic adenosine monophosphate response element–binding protein) that underlies learning and memory (*8*, *61*, *62*). Loss of this transcriptional program may be a cause for the synaptic and electrophysiological alterations we observed (*4*).

Dysfunctional Reelin signaling in human disease has been implicated in schizophrenia, where about 50% reduction of Reelin due to hypermethylation of the promoter region has been reported (*8*, *63*). Heterozygous *reeler* mice and human schizophrenic patients display reduced PPI, a defect not present in

the cKO mice. These animals showed a small increase in PPI, which points to a developmental origin for the schizophrenia caused by Reelin deficiency.

Impairment of Reelin signaling has been implicated in the cognitive impairment that manifests itself in AD. Patients with AD have alterations in Reelin abundance and glycosylation (*64*), and disease-associated single-nucleotide polymorphisms (SNPs) have been identified in the *RELN* locus in female AD patients (*65*). Additionally, a genome-wide association study (GWAS) found an association between SNPs in *RELN* and a high Braak score (high plaque and tangle load) in cognitively normal individuals. Individuals with high Braak scores and normal cognition also have increased Reelin abundance (*66*). This correlation of increased Reelin abundance with increased AD pathology and lack of cognitive deficits could be an indirect effect of the *RELN* SNPs promoting AD pathology. However, on the basis of our finding that loss of Reelin accelerates cognitive decline in Tg2576 mice independent of AD pathology, we suggest that these *RELN* SNPs render neurons resistant to Aβ accumulation by increasing the bioavailability of Reelin.

ApoE4 is the primary genetic risk factor for AD (*1*). We have previously identified a direct synaptic role for ApoE4 in impairing the active recycling of the ApoE receptors Apoer2 and Vldlr, which also bind Reelin, to and from the synaptic surface through an unknown mechanism, which leaves neurons unable to respond effectively to Reelin signaling (*2*). Because ApoE4 also promotes AD pathogenesis through other mechanisms [for example, increasing inflammatory processes, increasing tau phosphorylation, and reducing clearance of Aβ (*67*)], we sought to isolate the effects of Reelin loss on the background of increasing Aβ accumulation, which occurs in the early stages of AD. To do this, we crossed our Reelin cKO mice with the Tg2576 AD mouse model line, which has a relatively slow rate of Aβ accumulation that starts around 4 months and a cognitive decline not occurring until old age (*42*). We studied these mice at 7 months of age, at a time when Aβ oligomers have started to appear, but no amyloid deposition or cognitive decline has occurred (*68*).

Previous studies of Reelin in mouse models of AD have shown that Reelin affects Aβ abundance and amyloid deposition (*15*, *40*). Aβ-overproducing mice that are haploinsufficient for Reelin show a more rapid deposition of amyloid plaques and uncharacteristically develop neurofibrillary tangles at 15 months of age (*40*). Typically, Aβ-overproducing mice that are not transgenic for human tau do not develop tangles. In addition, nonphysiological and ectopic overexpression of Reelin in APP/PS1 transgenic mice slows plaque deposition and rescues memory impairment on the novel object recognition task (*15*). We have shown that the loss of adult Reelin in the context of minimal Aβ overproduction did not accelerate plaque development despite severe impairments in memory formation. Our findings contrast with those of Pujadas *et al.*, who were using an artificial overexpression system and animals expressing Reelin in the wrong cell type, which precludes conclusions about the physiological functions of Reelin. As predicted by our earlier studies (*12*), overexpression of Reelin can strengthen the intrinsic synaptic defense mechanisms against Aβ-mediated suppression; however, simple overexpression of Reelin in vivo does not allow us to deduce whether Reelin is indeed important for controlling synapse function in the presence of physiological amounts of Aβ. Moreover, using a Reelin cKO mouse model that also produces low amounts of human Aβ, we have established an animal model that allows us to gauge the importance of this evolutionarily ancient signaling pathway in protecting against a prevalent neurodegenerative disease of humans. Whereas our findings do not exclude an effect of Reelin loss on amyloid abundance at later stages of disease progression, they do suggest that it is indeed impaired Reelin signaling, through resistance to Reelin signaling induced by ApoE4, by which ApoE4 sensitizes the synapse to damage by Aβ (*2*).

AD is a devastating neurodegenerative disorder that affects millions of people worldwide. Thus far, Aβ-directed therapeutics have proven unsuccessful in treating patients, suggesting that a novel therapeutic approach is called for. We have shown that reduction of Reelin signaling in the adult brain, as occurs in aging and in the presence of ApoE4, leaves neurons susceptible to toxic damage caused by Aβ. Our results suggest that protecting and promoting Reelin signaling could be an effective method to prevent AD. This opens a new avenue to the identification of new types of therapeutics that can enhance Reelin abundance or restore normal lipoprotein receptor–mediated signaling in ApoE4 carriers.

MATERIALS AND METHODS

Animals

B6.Cg-Tg(CAG-cre/Esr1)5Amc/J mice, which we referred to as CAG-Cre^{ERT2} mice, were obtained from The Jackson Laboratory (*21*). The B6.129S4-$^{Meox2tm1(cre)Sor}$/J mice, which we referred to as Meox-Cre, were provided by M. Tallquist (*24*). Tg2576 mice were obtained from Taconic (*38*). Animals were group-housed in a standard 12-hour light cycle and fed standard mouse chow ad libitum. All animal care protocols were done in accordance with the Institutional Animal Care and Use Committee of the University of Texas Southwestern Medical Center and the University of Freiburg.

In light of the complexity of the genetic crosses and the different origins of the animal strains involved in this study, it has not been possible to conduct all experiments on a strictly homogenous C57Bl/6 strain background. To ensure a minimal effect of strain background on the behavioral results we have found, all animals that were compared were brother/sister crosses that only differ by the absence or presence of Cre recombinase. Moreover, discovering a robust response like the one discussed here in a mixed background, as opposed to an inbred one, further strengthens the validity of the conclusions, rather than diminishing them. It also further supports the applicability of the results to the even more genetically heterogeneous human population.

Generation of the *Reln$^{flox/flox}$* mouse

To create the targeting vector for the Reelin cKO mouse line, pJB1 [described in (*69*)] was used as background vector, and murine SV129J embryonic stem (ES) cell DNA was used as template DNA to amplify the short homology arm (SA; 1.35 kb), the fragment containing the first exon (EX1; 1.25 kb), and the long homology arm (LA; 9 kb). To incorporate the first loxP site, a Cla I and a Pvu I restriction site were included in the SA reverse and the EX1 forward primers, respectively. By three-fragment ligation, the (i) SA (cut with Sal I and Cla I) and (ii) EX1 (cut with Sal I and Pvu I) fragments were combined by a (iii) loxP coding linker (two annealed oligos with sticky ends for Cla I and Pvu I) and cloned between the Neo and HSVTK selection marker genes (Xho I site, compatible ends with Sal I) of pJB1. The resulting vector was opened with Not I to insert the 9-kb LA fragment 3′ downstream of the loxP/FRT-flanked neo cassette. The primers used were as follows: SA_forward, 5′- ATCGATGTCGACGGAAGTTTTGCTTCTTCCGGTG-3′ (Sal I); SA_reverse, 5′-CAATCGATGTTGTTTGTCTACGCCGGCTGCAAC-3′ (Cla I); EX1_forward, 5′-CCTTCTCGCGATCGCGCGTCCTCGCAGAACGGGCAGCC-3′ (Pvu I); EX1_reverse, 5′-GCGGCCGCGTCGACTGGGCAGCCACCGACCAAAGTGCTC-3′ (Sal I); LA_forward, 5′-TGTTGCGGCCGCGGCGGCCAGTTAAAAGTTCCCGCTG-3′ (Not I); LA_reverse, 5′-GTCGACGCGGCCGCTTCCATAAAAGGGAAGAGCAAGATG-3′ (Not I). The oligos used were loxP_forward, 5′-CGATAACTTCGTATAGCATACATTATACGAAGTTATAT-3′, and loxP_reverse, 5′-CGATATAACTTCGTATAATGTATGCTATACGAAGTTATCGAT-3′.

The final construct containing the SA-loxP-EX1-loxP-Neo-loxP-LA-HSVTK cassette was linearized and electroporated into SV129J ES cells. Gene

targeting–positive ES cells [polymerase chain reaction (PCR) screen] were injected into C57Bl/6J blastocysts, resulting in chimeric mice. The chimeras were crossed to C57Bl/6J mice, resulting in *Reln*$^{fl/wt}$ mice, verified by PCR and Southern blot. Heterozygous animals were backcrossed to Meox-Cre on the BL6 background to yield germline mutant *reeler* mice. Heterozygous animals were also backcrossed to CAG-^{CreERT2} mice to obtain homozygous *Reln*$^{fl/fl}$;*CAG-Cre* mice. These were again backcrossed to Tg2576 mice, and offspring used in the experiments were brother/sister crossed CAG-Cre hemizygous and Tg2576 hemizygous mice. To ensure a minimal effect on the behavioral results we have found, all animals that were compared were brother/sister crosses that differed only by the absence or presence of Cre recombinase.

Tamoxifen injections

At 2 months of age, mice were given daily intraperitoneal injections for 5 days of tamoxifen (135 mg/kg; Sigma) dissolved in sunflower oil. Control mice were injected with sunflower oil vehicle.

Antibodies

The following primary antibodies were used for the described experiments: NeuN (Millipore, Mab377; 1:300), NMDAR2B (Cell Signaling, 4212S; 1:2000), NR2A (Cell Signaling, 4205S; 1:500), GluR1 (Abcam, ab7260; 1:2000), GluR2/3 (Millipore, 07-598; 1:2000), β-actin (Abcam, ab8227; 1:3000), G10 [(*70*); 1:1000 for Western blotting, 1:500 for immunohistochemistry], 6E10 (Covance, SIG-39320), 4G8 (Covance, SIG-39220), Dab1 [5091 (*71*); 1:1000], phospho-GSK3β (Cell Signaling, 9336S; 1:3000), GSK3β (BD Transduction, 610201; 1:3000), phospho-Tau (Thr^{231}) (Invitrogen, 44746G; 1:5000), AT8 (Thermo, #MN1020; 1:2000), Tau-5 (Invitrogen, AHB0042; 1:5000), phospho-Akt (Ser^{473}) (Cell Signaling, 9271S; 1:1000), Akt (Cell Signaling, 9272S; 1:1000), phospho-ERK (Cell Signaling, 4370; 1:1000), ERK (Cell Signaling, 4696S; 1:1000), phospho-Src (Biosource, 44660; 1:1000), Src (Biosource, 44-656Z; 1:1000), and receptor-associated protein (RAP) (692, 1:1000). Secondary antibodies used were goat anti-mouse Alexa Fluor 488 (Molecular Probes, 1:1000, for immunohistochemistry), donkey anti-rabbit ECL, horseradish peroxidase (HRP)–linked (Amersham, NA934; 1:3000), and donkey anti-mouse 800 and donkey anti-rabbit 680 (LI-COR, 1:3000, for Western blotting).

Western blotting

Mice were deeply anesthetized with isoflurane and decapitated, and the hippocampi and cortices were rapidly dissected on ice. Tissues were immediately flash-frozen in liquid nitrogen. The tissue was homogenized in radioimmunoprecipitation assay buffer [50 mM tris (pH 8.0), 150 mM NaCl, 0.1% SDS, 0.5% sodium deoxycholate, 1% NP40] with protease and phosphatase inhibitors and then centrifuged at 14,000 rpm for 15 min to remove debris and nuclei. To analyze tau protein, tissues were homogenized in buffer [0.1 M MES (pH 6.8), 0.5 mM $MgSO_4$, 1 mM EGTA, 2 mM dithiothreitol, 0.5 M NaCl, 2 mM phenylmethylsulfonyl fluoride, 20 mM sodium fluoride, 0.5 mM sodium orthovanadate, 1 mM benzamidine, 25 mM β-glycerophosphate, 10 mM *p*-nitrophenylphosphate, aprotinin (10 μg/ml), leupeptin (10 μg/ml), 1 μM okadaic acid] and then clarified at 14,000 rpm for 5 min at 4°C. The supernatant was boiled for 5 min in a water bath and then put on ice for 5 min; the precipitated proteins were removed by centrifugation 14,000 rpm for 5 min. The supernatant was saved for analysis, as previously described (*3*). Protein concentration was determined using the Bio-Rad DC Protein Assay. Ten micrograms of protein was resolved on 4 to 15% Bio-Rad polyacrylamide gels and then transferred onto nitrocellulose membranes. The membranes were blocked in Odyssey (LI-COR) blocking buffer for 1 hour at room temperature and then incubated overnight in primary antibody. The membranes were protected from light and incubated with 1:3000 Odyssey secondary antibodies and then imaged on the Odyssey CLx Infrared Imaging System. Phosphorylated Src was quantified using ECL secondary antibody and developed using the SuperSignal West Femto Maximum Sensitivity Substrate because of low signal (Life Technologies). Blot quantification was performed using Image Studio software.

Behavioral characterization

All animals were allowed to acclimate in their home cage in the behavior facility for at least 1 hour before experimentation. Experiments were performed between 1400 and 1800. After completion of behavioral studies, Reelin knockout was confirmed by Western blot, and cKO mice that did not show greater than 95% reduction of Reelin in the forebrain were removed from data analysis.

Rotarod

Mice were placed on a Rotamex rotarod apparatus facing away from the experimenter. The rod was initially rotating at 2 rpm and then accelerated at a rate of 1 rpm/5 s until the mice fell off the rod or 300 s had passed. The time to falling off or the first "spin," when the mouse completed a full rotation holding on to the rod, ended the trial. The mice received four trials per day over the course of 10 days with a 15-min inter-trial interval. The slowest of the four trials was excluded, and the remaining three trials were averaged.

Open field

Mice were individually placed in the center of a VersaMax animal activity monitor, which contained a 42 cm × 42 cm acrylic box with a small layer of bedding. Activity was measured by beam breaks over the course of 60 min in bins of 2 min each. Movement was analyzed using the VersaDat analysis software.

Elevated plus maze

Mice were placed at the center of the elevated plus maze, which consisted of two open arms and two closed arms. Mice were allowed to explore the maze for 5 min, and the time spent in each arm was scored automatically.

Prepulse inhibition

Mice were placed in an SR-LAB startle response system. After 5-min acclimation to a background 70-dB noise, the mice first received five 120-dB tones to record baseline startle. They were then given a series of pseudo-random pairings of a 120-dB tone immediately preceded by a 0-, 74-, 78-, or 86-dB tone. PPI was calculated as the percentage of the average startle at each decibel over the average startle at 0 dB (no tone). After PPI training, mice were tested for startle amplitude over a range of decibels from 70 to 120 dB.

Morris water maze

Mice received a 2-day pretraining before Morris water maze in which they were placed in a small tub (30.5 cm × 61 cm) to find a fixed, hidden platform. They received eight trials per day in which they were given 30 s to find the platform. Mice who did not reach the platform within 10 s for six of eight trials on the second day did not proceed to the Morris water maze. More than 95% of the mice passed the pretraining. For the Morris water maze, mice were placed in a 120-cm-diameter pool that was made opaque with white washable paint. A 10-cm-diameter platform was placed in the center of the northeast ("target") quadrant of the pool, 1 cm under the surface of the water. Mice were placed in the pool starting in each of the four ordinary (N, S, E, W) directions in a pseudo-random order. A mouse was allowed 60 s to find the platform, and if unsuccessful, they were guided to the platform by the experimenter. After reaching the platform, mice remained there for 5 s before removal from the pool. Four trials happened per

day, with a 5-min inter-trial interval. Mice were trained for a total of 10 days. On day 11, the platform was removed for the probe trial, in which the mice swam in the pool for 60 s, and the time spent in each quadrant was recorded. On day 12, the platform was moved to the southeast corner, and its location was made obvious using a flag for the visible probe trial. Mouse movements were recorded and analyzed by the HVS Water software (HVS Image).

Fear conditioning

On day 1, mice were placed in a shock chamber for a 6-min training period, during the last 3 min of which they were exposed to three pairings of a 20-s shock followed by a 2-s 0.6-mA shock. On day 2, mice were placed in the chamber without the tone for 3 min, and the extent of freezing was recorded. Four hours later, mice were placed in a different context for 7 min, and during the last 4 min, they received three exposures to the tone. Mouse freezing was recorded with the FreezeFrame program and analyzed using the FreezeView program (Actimetrics).

Histology and immunohistochemistry

Mice were sacrificed with isoflurane and perfused with 20 ml of ice-cold PBS followed by 20 ml of ice-cold 4% paraformaldehyde (PFA) in PBS. Brains were removed and postfixed in 4% PFA overnight at 4°C. Brains were immobilized in 5% agarose in PBS, and 50-μm-thick sections were sliced on a Leica VT1000 S vibratome. Sections were stored in 0.02% sodium azide in PBS at 4°C. For cresyl violet staining, sections were mounted on charged slides and dried at room temperature overnight. Slides were serially placed in 100% ethanol, 95% ethanol, and double-distilled water, and then stained in 0.1% cresyl violet. Slides were destained in 95% ethanol, then placed in 100% ethanol and xylene, and mounted. NeuN and Reelin immunohistochemistry was done by blocking slices in 3% goat serum for 3 hours at 4°C, then overnight in 1:300 NeuN or 1:500 G10 antibody. Alexa Fluor 594 goat anti-mouse secondary antibody was applied for 2 hours at room temperature, and then hippocampi were imaged at 20× for NeuN. Sequential images of the anti-Reelin sections were acquired using a 10× objective and stitched together using Microsoft Image Composite Editor. For Aβ immunostaining, sections were blocked in 3% H_2O_2 in methanol for 20 min, followed by 88% formic acid pretreatment for 3 min. The sections were blocked for 2 hours at room temperature with tris-buffered saline (TBS) containing 10% normal horse serum, 2% DL-lysine, 0.25% Triton-X, and a Fab mouse immunoglobulin G (IgG) (H&L) antibody fragment of anti-mouse IgG (1:1000; Rockland Immunochemicals Inc.). Aβ was detected with the antibody 4G8 (1:1000; Covance) followed by incubation with biotinylated anti-mouse IgG secondary antibody. Bound antibodies were visualized by using an ABC (avidin-biotin complex) kit (Vector Laboratories) and a diaminobenzidine kit (Sigma).

Golgi staining

Golgi staining was performed using the FD Rapid GolgiStain Kit (FD Neurotechnologies) according to the manufacturer's instructions. Slices of 200-μm thickness were obtained with a vibratome (*4*). Z-sections of the Golgi-stained brains were acquired to measure the spine density of CA1 apical dendrites. Images were zoomed in 4× to measure the height and width of the spines.

Granule cell dispersion

Six serial sections of dorsal hippocampus were taken from each fixed brain and stained with cresyl violet. Images were taken at 20×. The length of the dentate gyrus was divided into 100-μm segments, and at the center of each segment, the width was measured. The average width per animal was taken for each *n*.

Aβ quantification

Protein extraction from fresh-frozen mouse forebrain (0.4 g) was carried out in 1 ml of 1× TBS containing protease and phosphatase inhibitors. The tissue was homogenized with a micropestle (Eppendorf) followed by sonication. The homogenate was centrifuged for 30 min at 14,000*g* at 4°C. The supernatant (soluble fraction) was transferred into fresh tubes and kept at −80°C until further use. The remaining pellet was resuspended in 1 ml of PBS containing 1% Triton-X followed by sonication and centrifugation as previously mentioned. For the Aβ ELISA, the tissue was homogenized in PBS and then centrifuged at 14,000 rpm for 25 min at 4°C. The supernatant was reserved (soluble fraction), and the pellet was homogenized in 0.5 M guanidine, allowed to solubilize for 3 hours, and then spun at 14,000 rpm for 25 min (insoluble fraction). A sandwich ELISA was performed using antibodies donated by D. Holtzman. Briefly, Nunc MaxiSorp (Thermo) plates were coated with either HJ2 (anti-$Aβ_{40}$) or HJ7.4 (anti-$Aβ_{42}$) and incubated overnight at 4°C. Plates were then incubated with blocking buffer for 1.5 hours. Plates were incubated overnight with the soluble and insoluble tissue samples. The plates were then incubated with HJ5.1-biotin, which recognizes both forms of Aβ. The plates were coated with streptavidin–poly-HRP40 (Pierce) and then developed with Super Slow 3,3′,5,5′-tetramethylbenzidine (Sigma).

Field electrophysiology and θ-burst LTP

θ-Burst LTP was performed as previously described (*2*). Briefly, mice were deeply anesthetized with isoflurane, and their brains were quickly removed and placed in ice-cold high-sucrose slicing solution (110 mM sucrose, 60 mM NaCl, 3 mM KCl, 1.25 mM NaH_2PO_4, 28 mM $NaHCO_3$, 0.5 mM $CaCl_2$, 5 mM glucose, 0.6 mM ascorbic acid, 7 mM $MgSO_4$). Transverse slices (350 μm) were cut using a Leica VT1000S vibratome. Slices were allowed to recover in ACSF (124 mM NaCl, 3 mM KCl, 1.25 mM NaH_2PO_4, 26 mM $NaHCO_3$, 10 mM D-glucose, 2 mM $CaCl_2$, 1 mM $MgSO_4$) for 1 hour at room temperature before the experiments. For recording, slices were transferred to an interface chamber perfused with ACSF at 31°C. Slices were stimulated in the stratum radiatum with concentric bipolar electrodes (FHC) using an isolated pulse stimulator. The stimulus intensity was set to 40 to 60% of the maximum peak amplitude, as determined by measuring the input-output curve. After the baseline stabilized, a θ-burst was applied using a train of four 100-Hz pulses repeated 10 times with 200-ms intervals, and the train was repeated five times at 10-s intervals. The resulting LTP was measured for 1 hour after θ-burst stimulation. Data were analyzed using LabView 7.0.

Statistical analysis

Data were analyzed with GraphPad Prism software (version 6.0, GraphPad Software). Data are shown as means ± SEM, and statistical significance was set at $P < 0.05$.

SUPPLEMENTARY MATERIALS

www.sciencesignaling.org/cgi/content/full/8/384/ra67/DC1
Fig. S1. Brain-wide Reelin knockout in Reelin cKO mice.
Fig. S2. Meox-Cre–driven Reelin knockout results in a *reeler* phenotype.
Fig. S3. Behavioral findings in Reelin cKO mice.
Fig. S4. Morris water maze in 7-month-old cKO mice.

REFERENCES AND NOTES

1. E. H. Corder, A. M. Saunders, W. J. Strittmatter, D. E. Schmechel, P. C. Gaskell, G. W. Small, A. D. Roses, J. L. Haines, M. A. Pericak-Vance, Gene dose of apolipoprotein E type 4 allele and the risk of Alzheimer's disease in late onset families. *Science* **261**, 921–923 (1993).
2. Y. Chen, M. S. Durakoglugil, X. Xian, J. Herz, ApoE4 reduces glutamate receptor function and synaptic plasticity by selectively impairing ApoE receptor recycling. *Proc. Natl. Acad. Sci. U.S.A.* **107**, 12011–12016 (2010).

3. T. Hiesberger, M. Trommsdorff, B. W. Howell, A. Goffinet, M. C. Mumby, J. A. Cooper, J. Herz, Direct binding of Reelin to VLDL receptor and ApoE receptor 2 induces tyrosine phosphorylation of disabled-1 and modulates tau phosphorylation. *Neuron* **24**, 481–489 (1999).
4. C. R. Wasser, I. Masiulis, M. S. Durakoglugil, C. Lane-Donovan, X. Xian, U. Beffert, A. Agarwala, R. E. Hammer, J. Herz, Differential splicing and glycosylation of Apoer2 alters synaptic plasticity and fear learning. *Sci. Signal.* **7**, ra113 (2014).
5. V. Strasser, D. Fasching, C. Hauser, H. Mayer, H. H. Bock, T. Hiesberger, J. Herz, E. J. Weeber, J. D. Sweatt, A. Pramatarova, B. Howell, W. J. Schneider, J. Nimpf, Receptor clustering is involved in Reelin signaling. *Mol. Cell. Biol.* **24**, 1378–1386 (2004).
6. U. Beffert, G. Morfini, H. H. Bock, H. Reyna, S. T. Brady, J. Herz, Reelin-mediated signaling locally regulates protein kinase B/Akt and glycogen synthase kinase 3β. *J. Biol. Chem.* **277**, 49958–49964 (2002).
7. H. H. Bock, J. Herz, Reelin activates SRC family tyrosine kinases in neurons. *Curr. Biol.* **13**, 18–26 (2003).
8. D. R. Grayson, X. Jia, Y. Chen, R. P. Sharma, C. P. Mitchell, A. Guidotti, E. Costa, Reelin promoter hypermethylation in schizophrenia. *Proc. Natl. Acad. Sci. U.S.A.* **102**, 9341–9346 (2005).
9. M. A. Takasu, M. B. Dalva, R. E. Zigmond, M. E. Greenberg, Modulation of NMDA receptor-dependent calcium influx and gene expression through EphB receptors. *Science* **295**, 491–495 (2002).
10. E. M. Snyder, Y. Nong, C. G. Almeida, S. Paul, T. Moran, E. Y. Choi, A. C. Nairn, M. W. Salter, P. J. Lombroso, G. K. Gouras, P. Greengard, Regulation of NMDA receptor trafficking by amyloid-β. *Nat. Neurosci.* **8**, 1051–1058 (2005).
11. E. J. Weeber, U. Beffert, C. Jones, J. M. Christian, E. Forster, J. D. Sweatt, J. Herz, Reelin and ApoE receptors cooperate to enhance hippocampal synaptic plasticity and learning. *J. Biol. Chem.* **277**, 39944–39952 (2002).
12. M. S. Durakoglugil, Y. Chen, C. L. White, E. T. Kavalali, J. Herz, Reelin signaling antagonizes β-amyloid at the synapse. *Proc. Natl. Acad. Sci. U.S.A.* **106**, 15938–15943 (2009).
13. D. M. Walsh, I. Klyubin, J. V. Fadeeva, W. K. Cullen, R. Anwyl, M. S. Wolfe, M. J. Rowan, D. J. Selkoe, Naturally secreted oligomers of amyloid β protein potently inhibit hippocampal long-term potentiation in vivo. *Nature* **416**, 535–539 (2002).
14. J. T. Rogers, I. Rusiana, J. Trotter, L. Zhao, E. Donaldson, D. T. Pak, L. W. Babus, M. Peters, J. L. Banko, P. Chavis, G. W. Rebeck, H. S. Hoe, E. J. Weeber, Reelin supplementation enhances cognitive ability, synaptic plasticity, and dendritic spine density. *Learn. Mem.* **18**, 558–564 (2011).
15. L. Pujadas, D. Rossi, R. Andrés, C. M. Teixeira, B. Serra-Vidal, A. Parcerisas, R. Maldonado, E. Giralt, N. Carulla, E. Soriano, Reelin delays amyloid-β fibril formation and rescues cognitive deficits in a model of Alzheimer's disease. *Nat. Commun.* **5**, 3443 (2014).
16. G. D'Arcangelo, R. Homayouni, L. Keshvara, D. S. Rice, M. Sheldon, T. Curran, Reelin is a ligand for lipoprotein receptors. *Neuron* **24**, 471–479 (1999).
17. G. D'Arcangelo, G. G. Miao, S. C. Chen, H. D. Soares, J. I. Morgan, T. Curran, A protein related to extracellular matrix proteins deleted in the mouse mutant *reeler*. *Nature* **374**, 719–723 (1995).
18. D. S. Falconer, Two new mutants, "trembler" and "reeler", with neurological actions in the house mouse (*Mus musculus* L.). *J. Genet.* **50**, 192–201 (1951).
19. S. Qiu, K. M. Korwek, A. R. Pratt-Davis, M. Peters, M. Y. Bergman, E. J. Weeber, Cognitive disruption and altered hippocampus synaptic function in Reelin haploinsufficient mice. *Neurobiol. Learn. Mem.* **85**, 228–242 (2006).
20. P. Tueting, E. Costa, Y. Dwivedi, A. Guidotti, F. Impagnatiello, R. Manev, C. Pesold, The phenotypic characteristics of heterozygous reeler mouse. *Neuroreport* **10**, 1329–1334 (1999).
21. S. Hayashi, A. P. McMahon, Efficient recombination in diverse tissues by a tamoxifen-inducible form of Cre: A tool for temporally regulated gene activation/inactivation in the mouse. *Dev. Biol.* **244**, 305–318 (2002).
22. L. Arnaud, B. A. Ballif, E. Förster, J. A. Cooper, Fyn tyrosine kinase is a critical regulator of Disabled-1 during brain development. *Curr. Biol.* **13**, 9–17 (2003).
23. H. H. Bock, Y. Jossin, P. May, O. Bergner, J. Herz, Apolipoprotein E receptors are required for Reelin-induced proteasomal degradation of the neuronal adaptor protein Disabled-1. *J. Biol. Chem.* **279**, 33471–33479 (2004).
24. M. D. Tallquist, P. Soriano, Epiblast-restricted Cre expression in MORE mice: A tool to distinguish embryonic vs. extra-embryonic gene function. *Genesis* **26**, 113–115 (2000).
25. J. Trotter, G. H. Lee, T. M. Kazdoba, B. Crowell, J. Domogauer, H. M. Mahoney, S. J. Franco, U. Müller, E. J. Weeber, G. D'Arcangelo, Dab1 is required for synaptic plasticity and associative learning. *J. Neurosci.* **33**, 15652–15668 (2013).
26. G. H. Lee, Z. Chhangawala, S. von Daake, J. N. Savas, J. R. Yates III, D. Comoletti, G. D'Arcangelo, Reelin induces Erk1/2 signaling in cortical neurons through a non-canonical pathway. *J. Biol. Chem.* **289**, 20307–20317 (2014).
27. T. Isosaka, K. Hattori, T. Yagi, NMDA-receptor proteins are upregulated in the hippocampus of postnatal heterozygous *reeler* mice. *Brain Res.* **1073–1074**, 11–19 (2006).
28. J. Brich, F. S. Shie, B. W. Howell, R. Li, K. Tus, E. K. Wakeland, L. W. Jin, M. Mumby, G. Churchill, J. Herz, J. A. Cooper, Genetic modulation of tau phosphorylation in the mouse. *J. Neurosci.* **23**, 187–192 (2003).
29. C. A. Haas, M. Frotscher, Reelin deficiency causes granule cell dispersion in epilepsy. *Exp. Brain Res.* **200**, 141–149 (2010).
30. C. Heinrich, N. Nitta, A. Flubacher, M. Müller, A. Fahrner, M. Kirsch, T. Freiman, F. Suzuki, A. Depaulis, M. Frotscher, C. A. Haas, Reelin deficiency and displacement of mature neurons, but not neurogenesis, underlie the formation of granule cell dispersion in the epileptic hippocampus. *J. Neurosci.* **26**, 4701–4713 (2006).
31. E. Bouché, M. I. Romero-Ortega, M. Henkemeyer, T. Catchpole, J. Leemhuis, M. Frotscher, P. May, J. Herz, H. H. Bock, Reelin induces EphB activation. *Cell Res.* **23**, 473–490 (2013).
32. N. Utsunomiya-Tate, K. Kubo, S. Tate, M. Kainosho, E. Katayama, K. Nakajima, K. Mikoshiba, Reelin molecules assemble together to form a large protein complex, which is inhibited by the function-blocking CR-50 antibody. *Proc. Natl. Acad. Sci. U.S.A.* **97**, 9729–9734 (2000).
33. L. Dulabon, E. C. Olson, M. G. Taglienti, S. Eisenhuth, B. McGrath, C. A. Walsh, J. A. Kreidberg, E. S. Anton, Reelin binds α3β1 integrin and inhibits neuronal migration. *Neuron* **27**, 33–44 (2000).
34. S. Niu, O. Yabut, G. D'Arcangelo, The Reelin signaling pathway promotes dendritic spine development in hippocampal neurons. *J. Neurosci.* **28**, 10339–10348 (2008).
35. J. T. Rogers, L. Zhao, J. H. Trotter, I. Rusiana, M. M. Peters, Q. Li, E. Donaldson, J. L. Banko, K. E. Keenoy, G. W. Rebeck, H. S. Hoe, G. D'Arcangelo, E. J. Weeber, Reelin supplementation recovers sensorimotor gating, synaptic plasticity and associative learning deficits in the heterozygous reeler mouse. *J. Psychopharmacol.* **27**, 386–395 (2013).
36. J. Podhorna, M. Didriksen, The heterozygous reeler mouse: Behavioural phenotype. *Behav. Brain Res.* **153**, 43–54 (2004).
37. E. Ognibene, W. Adriani, O. Granstrem, S. Pieretti, G. Laviola, Impulsivity–anxiety-related behavior and profiles of morphine-induced analgesia in heterozygous reeler mice. *Brain Res.* **1131**, 173–180 (2007).
38. K. Hsiao, P. Chapman, S. Nilsen, C. Eckman, Y. Harigaya, S. Younkin, F. Yang, G. Cole, Correlative memory deficits, Aβ elevation, and amyloid plaques in transgenic mice. *Science* **274**, 99–102 (1996).
39. M. N. Gordon, D. L. King, D. M. Diamond, P. T. Jantzen, K. V. Boyett, C. E. Hope, J. M. Hatcher, G. DiCarlo, W. P. Gottschall, D. Morgan, G. W. Arendash, Correlation between cognitive deficits and Aβ deposits in transgenic APP+PS1 mice. *Neurobiol. Aging* **22**, 377–385 (2001).
40. S. Kocherhans, A. Madhusudan, J. Doehner, K. S. Breu, R. M. Nitsch, J. M. Fritschy, I. Knuesel, Reduced Reelin expression accelerates amyloid-β plaque formation and tau pathology in transgenic Alzheimer's disease mice. *J. Neurosci.* **30**, 9228–9240 (2010).
41. K. S. Kim, D. M. Miller, V. J. Sapienza, C. J. Chen, C. Bai, I. Grundke-Iqbal, J. R. Currie, W. H. M., Production and characterization of monoclonal antibodies reactive to synthetic cerebrovascular amyloid peptide. *Neurosci. Res. Commun.* **2**, 121–130 (1988).
42. T. Kawarabayashi, L. H. Younkin, T. C. Saido, M. Shoji, K. H. Ashe, S. G. Younkin, Age-dependent changes in brain, CSF, and plasma amyloid β protein in the Tg2576 transgenic mouse model of Alzheimer's disease. *J. Neurosci.* **21**, 372–381 (2001).
43. H. S. Hoe, K. J. Lee, R. S. Carney, J. Lee, A. Markova, J. Y. Lee, B. W. Howell, B. T. Hyman, D. T. Pak, G. Bu, G. W. Rebeck, Interaction of Reelin with amyloid precursor protein promotes neurite outgrowth. *J. Neurosci.* **29**, 7459–7473 (2009).
44. C. Leeb, C. Eresheim, J. Nimpf, Clusterin is a ligand for apolipoprotein E receptor 2 (ApoER2) and very low density lipoprotein receptor (VLDLR) and signals via the Reelin-signaling pathway. *J. Biol. Chem.* **289**, 4161–4172 (2014).
45. D. H. Kim, H. Iijima, K. Goto, J. Sakai, H. Ishii, H. J. Kim, H. Suzuki, H. Kondo, S. Saeki, T. Yamamoto, Human apolipoprotein E receptor 2: A novel lipoprotein receptor of the low density lipoprotein receptor family predominantly expressed in brain. *J. Biol. Chem.* **271**, 8373–8380 (1996).
46. H. S. Hoe, D. Wessner, U. Beffert, A. G. Becker, Y. Matsuoka, G. W. Rebeck, F-spondin interaction with the apolipoprotein E receptor ApoEr2 affects processing of amyloid precursor protein. *Mol. Cell. Biol.* **25**, 9259–9268 (2005).
47. M. Trommsdorff, J. P. Borg, B. Margolis, J. Herz, Interaction of cytosolic adaptor proteins with neuronal apolipoprotein E receptors and the amyloid precursor protein. *J. Biol. Chem.* **273**, 33556–33560 (1998).
48. R. S. Schmid, R. Jo, S. Shelton, J. A. Kreidberg, E. S. Anton, Reelin, integrin and Dab1 interactions during embryonic cerebral cortical development. *Cereb. Cortex* **15**, 1632–1636 (2005).
49. O. Y. Kwon, K. Hwang, J. A. Kim, K. Kim, I. C. Kwon, H. K. Song, H. Jeon, Dab1 binds to Fe65 and diminishes the effect of Fe65 or LRP1 on APP processing. *J. Cell. Biochem.* **111**, 508–519 (2010).
50. R. Homayouni, D. S. Rice, M. Sheldon, T. Curran, Disabled-1 binds to the cytoplasmic domain of amyloid precursor-like protein 1. *J. Neurosci.* **19**, 7507–7515 (1999).
51. J. C. Lambert, S. Heath, G. Even, D. Campion, K. Sleegers, M. Hiltunen, O. Combarros, D. Zelenika, M. J. Bullido, B. Tavernier, L. Letenneur, K. Bettens, C. Berr, F. Pasquier, N. Fiévet, P. Barberger-Gateau, S. Engelborghs, P. De Deyn, I. Mateo, A. Franck, S. Helisalmi, E. Porcellini, O. Hanon; I. European Alzheimer's Disease Initiative, M. M. de Pancorbo, C. Lendon, C. Dufouil, C. Jaillard, T. Leveillard, V. Alvarez, P. Bosco, M. Mancuso, F. Panza, B. Nacmias, P. Bossù, P. Piccardi, G. Annoni, D. Seripa, D. Galimberti, D. Hannequin, F. Licastro, H. Soininen, K. Ritchie, H. Blanché, J. F. Dartigues, C. Tzourio, I. Gut,

C. Van Broeckhoven, A. Alpérovitch, M. Lathrop, P. Amouyel, Genome-wide association study identifies variants at *CLU* and *CR1* associated with Alzheimer's disease. *Nat. Genet.* **41**, 1094–1099 (2009).
52. C. R. Houser, Granule cell dispersion in the dentate gyrus of humans with temporal lobe epilepsy. *Brain Res.* **535**, 195–204 (1990).
53. F. Suzuki, M. P. Junier, D. Guilhem, J. C. Sørensen, B. Onteniente, Morphogenetic effect of kainate on adult hippocampal neurons associated with a prolonged expression of brain-derived neurotrophic factor. *Neuroscience* **64**, 665–674 (1995).
54. M. C. Müller, M. Osswald, S. Tinnes, U. Häussler, A. Jacobi, E. Förster, M. Frotscher, C. A. Haas, Exogenous reelin prevents granule cell dispersion in experimental epilepsy. *Exp. Neurol.* **216**, 390–397 (2009).
55. X. Chai, G. Münzner, S. Zhao, S. Tinnes, J. Kowalski, U. Häussler, C. Young, C. A. Haas, M. Frotscher, Epilepsy-induced motility of differentiated neurons. *Cereb. Cortex* **24**, 2130–2140 (2014).
56. K. M. Korwek, J. H. Trotter, M. J. Ladu, P. M. Sullivan, E. J. Weeber, ApoE isoform-dependent changes in hippocampal synaptic function. *Mol. Neurodegener.* **4**, 21 (2009).
57. J. Levenga, P. Krishnamurthy, H. Rajamohamedsait, H. Wong, T. F. Franke, P. Cain, E. M. Sigurdsson, C. A. Hoeffer, Tau pathology induces loss of GABAergic interneurons leading to altered synaptic plasticity and behavioral impairments. *Acta Neuropathol. Commun.* **1**, 34 (2013).
58. L. Groc, D. Choquet, F. A. Stephenson, D. Verrier, O. J. Manzoni, P. Chavis, NMDA receptor surface trafficking and synaptic subunit composition are developmentally regulated by the extracellular matrix protein Reelin. *J. Neurosci.* **27**, 10165–10175 (2007).
59. M. Sinagra, D. Verrier, D. Frankova, K. M. Korwek, J. Blahos, E. J. Weeber, O. J. Manzoni, P. Chavis, Reelin, very-low-density lipoprotein receptor, and apolipoprotein E receptor 2 control somatic NMDA receptor composition during hippocampal maturation in vitro. *J. Neurosci.* **25**, 6127–6136 (2005).
60. Y. P. Tang, E. Shimizu, G. R. Dube, C. Rampon, G. A. Kerchner, M. Zhuo, G. Liu, J. Z. Tsien, Genetic enhancement of learning and memory in mice. *Nature* **401**, 63–69 (1999).
61. K. Zurhove, C. Nakajima, J. Herz, H. H. Bock, P. May, γ-Secretase limits the inflammatory response through the processing of LRP1. *Sci. Signal.* **1**, ra15 (2008).
62. F. Telese, Q. Ma, P. M. Perez, D. Notani, S. Oh, W. Li, D. Comoletti, K. A. Ohgi, H. Taylor, M. G. Rosenfeld, *LRP8-Reelin-regulated neuronal enhancer signature underlying learning and memory formation. Neuron* **86**, 696–710 (2015).
63. F. Impagnatiello, A. R. Guidotti, C. Pesold, Y. Dwivedi, H. Caruncho, M. G. Pisu, D. P. Uzunov, N. R. Smalheiser, J. M. Davis, G. N. Pandey, G. D. Pappas, P. Tueting, R. P. Sharma, E. Costa, A decrease of reelin expression as a putative vulnerability factor in schizophrenia. *Proc. Natl. Acad. Sci. U.S.A.* **95**, 15718–15723 (1998).
64. A. Botella-López, F. Burgaya, R. Gavín, M. S. Garcia-Ayllón, E. Gómez-Tortosa, J. Peña-Casanova, J. M. Ureña, J. A. Del Río, R. Blesa, E. Soriano, J. Sáez-Valero, Reelin expression and glycosylation patterns are altered in Alzheimer's disease. *Proc. Natl. Acad. Sci. U.S.A.* **103**, 5573–5578 (2006).
65. D. Seripa, M. G. Matera, M. Franceschi, A. Daniele, A. Bizzarro, M. Rinaldi, F. Panza, V. M. Fazio, C. Gravina, G. D'Onofrio, V. Solfrizzi, C. Masullo, A. Pilotto, The RELN locus in Alzheimer's disease. *J. Alzheimers Dis.* **14**, 335–344 (2008).
66. P. L. Kramer, H. Xu, R. L. Woltjer, S. K. Westaway, D. Clark, D. Erten-Lyons, J. A. Kaye, K. A. Welsh-Bohmer, J. C. Troncoso, W. R. Markesbery, R. C. Petersen, R. S. Turner, W. A. Kukull, D. A. Bennett, D. Galasko, J. C. Morris, J. Ott, Alzheimer disease pathology in cognitively healthy elderly: A genome-wide study. *Neurobiol. Aging* **32**, 2113–2122 (2011).
67. D. M. Holtzman, J. Herz, G. Bu, Apolipoprotein E and apolipoprotein E receptors: Normal biology and roles in Alzheimer disease. *Cold Spring Harb. Perspect. Med.* **2**, a006312 (2012).
68. M. A. Westerman, D. Cooper-Blacketer, A. Mariash, L. Kotilinek, T. Kawarabayashi, L. H. Younkin, G. A. Carlson, S. G. Younkin, K. H. Ashe, The relationship between Aβ and memory in the Tg2576 mouse model of Alzheimer's disease. *J. Neurosci.* **22**, 1858–1867 (2002).
69. J. P. Braybrooke, K. G. Spink, J. Thacker, I. D. Hickson, The RAD51 family member, RAD51L3, is a DNA-stimulated ATPase that forms a complex with XRCC2. *J. Biol. Chem.* **275**, 29100–29106 (2000).
70. U. Beffert, A. Durudas, E. J. Weeber, P. C. Stolt, K. M. Giehl, J. D. Sweatt, R. E. Hammer, J. Herz, Functional dissection of Reelin signaling by site-directed disruption of Disabled-1 adaptor binding to apolipoprotein E receptor 2: Distinct roles in development and synaptic plasticity. *J. Neurosci.* **26**, 2041–2052 (2006).
71. M. Trommsdorff, M. Gotthardt, T. Hiesberger, J. Shelton, W. Stockinger, J. Nimpf, R. E. Hammer, J. A. Richardson, J. Herz, Reeler/Disabled-like disruption of neuronal migration in knockout mice lacking the VLDL receptor and ApoE receptor 2. *Cell* **97**, 689–701 (1999).

Acknowledgments: We would like to thank D. Holtzman for providing the Aβ antibodies used for the ELISA studies. **Funding:** This work was supported by NIH grants F30 AG047799 (to C.L.-D.) and R37 HL63762 (to J.H.), the American Health Assistance Foundation, the Consortium for Frontotemporal Dementia Research, the Bright Focus Foundation, the Lupe Murchison Foundation, and The Ted Nash Long Life Foundation. This work was also supported by Deutsche Forschungsgemeinschaft [DFG; grant numbers FR 620/12-1 (to M.F.) and SFB 780/TP5 (to J.H., H.H.B., and M.F.)] and Bundesministerium für Bildung und Forschung (BMBF, e:bio ReelinSys, to H.H.B.). M.F. is Senior Research Professor of the Hertie Foundation. **Author contributions:** C.L.-D., G.T.P., C.R.W., M.S.D., H.H.B., and J.H. designed the experiments. C.L.-D., G.T.P., C.R.W., M.S.D., A.U., T.P., L.S., and C.C. performed the experiments. L.S., T.P., T.K., R.E.H., and I.M. generated and validated the mouse model. C.L.-D. and J.H. prepared the manuscript. M.F., H.H.B., and J.H. supervised the project. **Competing interests:** The authors declare that they have no competing interests. **Data and materials availability:** The Reelin cKO mice require a material transfer agreement from the University of Texas Southwestern Medical Center.

Submitted 11 January 2015
Accepted 18 June 2015
Final Publication 7 July 2015
10.1126/scisignal.aaa6674
Citation: C. Lane-Donovan, G. T. Philips, C. R. Wasser, M. S. Durakoglugil, I. Masiulis, A. Upadhaya, T. Pohlkamp, C. Coskun, T. Kotti, L. Steller, R. E. Hammer, M. Frotscher, H. H. Bock, J. Herz, Reelin protects against amyloid β toxicity in vivo. *Sci. Signal.* **8**, ra67 (2015).

Science Signaling

Reelin protects against amyloid β toxicity in vivo

Courtney Lane-Donovan, Gary T. Philips, Catherine R. Wasser, Murat S. Durakoglugil, Irene Masiulis, Ajeet Upadhaya, Theresa Pohlkamp, Cagil Coskun, Tiina Kotti, Laura Steller, Robert E. Hammer, Michael Frotscher, Hans H. Bock and Joachim Herz

Sci. Signal. **8** (384), ra67.
DOI: 10.1126/scisignal.aaa6674

Protecting neurons from amyloid β

In the developing nervous system, the secreted protein Reelin helps to guide migrating neurons to their correct destination. In the adult nervous system, Reelin enhances synaptic plasticity and protects isolated neurons from the toxicity of amyloid β, the accumulation of which causes the neurodegeneration characteristic of Alzheimer's disease. To avoid the developmental defects associated with Reelin deficiency, Lane-Donovan *et al.* generated mice with an inducible knockout of Reelin that accumulated amyloid β. Mice that lacked Reelin as adults showed greater defects in synaptic plasticity, learning, and memory in response to amyloid β accumulation, indicating that Reelin protects against the neurotoxicity of amyloid β in vivo.

Science Signaling (ISSN 1937-9145) is published by the American Association for the Advancement of Science, 1200 New York Avenue NW, Washington, DC 20005. The title *Science Signaling* is a registered trademark of AAAS.

Science Signaling (ISSN 1937-9145) is published by the American Association for the Advancement of Science, 1200 New York Avenue NW, Washington, DC 20005. The title *Science Signaling* is a registered trademark of AAAS.